REPORT 1171

EFFECT OF HORIZONTAL-TAIL SPAN AND VERTICAL LOCATION ON THE AERODYNAMIC CHARACTERISTICS OF AN UNSWEPT TAIL ASSEMBLY IN SIDESLIP [1]

By Donald R. Riley

SUMMARY

An investigation has been conducted in the Langley stability tunnel on a vertical-tail model with a stub fuselage in combination with various horizontal tails to determine the effect of horizontal-tail span and vertical location of the horizontal tail relative to the vertical tail on the aerodynamic characteristics of an unswept tail assembly in sideslip.

The results of the investigation indicated that the induced loading carried by the horizontal tail produced a rolling moment about the point of attachment to the vertical tail which was strongly influenced by horizontal-tail span and vertical location. The greatest effect of horizontal-tail span on the rolling-moment derivative of the complete tail assembly was obtained for horizontal-tail locations near the top of the vertical tail.

The addition of a horizontal tail to the fuselage—vertical-tail combination produced the greatest increase in the magnitude of the lateral-force derivative when the horizontal tail was located near either tip of the vertical tail. Locating horizontal tails of all spans one-quarter and one-half of the vertical-tail span above the base of the vertical tail produced a decrease in the magnitude of the lateral-force derivative of the horizontal-tail-off configuration.

Span loadings which were reduced to the static-stability derivatives were calculated for each configuration tested by applying the well-known finite-step method used for wings to the intersecting surfaces of the vertical and horizontal tails. The method consists in replacing the vertical and horizontal tails by a finite number of horseshoe vortices having the bound portion located at the quarter-chord line. The stability derivatives obtained by this method were in good agreement with wind-tunnel results. The finite-step method provides a simple and effective means of investigating the span loadings of intersecting surfaces.

INTRODUCTION

The need to provide a more complete estimate of the tail contribution to the static lateral stability of complete airplane configurations and to provide a basis for structural considerations of the tail assembly, including the afterportion of the fuselage, has emphasized the lack of a complete theory from which could be obtained the span loadings for horizontal-tail and vertical-tail combinations in sideslip. A minimum-induced-drag solution for the effects of horizontal-tail span and vertical location on a centrally located vertical tail at an angle of sideslip was obtained in reference 1. A lifting-line solution (ref. 2) has been obtained for the one case of the horizontal tail located at the base of the vertical tail, elliptical and semielliptical plan forms and coinciding root chords being assumed. A comparison of the two solutions presented in reference 2 indicates that the implied infinite-chord horizontal tail of the minimum-induced-drag theory leads to an excessive end-plate effect for the range of tail sizes usually under consideration.

Several attempts, such as references 3 and 4, have been made to synthesize a solution by using the results of references 1 and 2. Reference 2 is used, in effect, to extrapolate the results of reference 1 to a finite horizontal-tail chord. These attempts have been concerned mainly with obtaining a reasonable estimate of the end-plate effect of the horizontal tail on the vertical-tail lift-curve slope. The rolling moment of the horizontal- and vertical-tail combination about the base of the vertical tail and the rolling moment of the horizontal tail about its point of attachment to the vertical tail have been treated only in references 1 and 2 and, as a result, only reasonable estimates can be obtained for the case of the horizontal tail located at the base of the vertical tail.

Since the available theories for calculating these aerodynamic characteristics are rather limited, an experimental investigation was conducted in the Langley stability tunnel to determine the effect of horizontal-tail span and vertical location on the aerodynamic characteristics of an unswept tail assembly in sideslip. In addition, the results serve to determine the applicability of the well-known discrete horseshoe-vortex solution for determining span loadings of wings to the problem of intersecting surfaces as a means of approximating the loading and, hence, the rolling moments. This finite-step method which can be considered as a simplified lifting-surface theory involves the use of n horseshoe vortices placed along the lifting line of the vertical and horizontal tails and the application of the boundary condition of zero velocity normal to the surface at the three-quarter-chord line for n spanwise stations; this method yields a system of n equations in n unknowns. Solutions of simultaneous equations of this type of high order are usually somewhat cumbersome to obtain by manually operated computing machines but are reasonably well adapted to the relay-type digital computing machines.

[1] Supersedes NACA TN 2907, "Effect of Horizontal-Tail Span and Vertical Location on the Aerodynamic Characteristics of an Unswept Tail Assembly in Sideslip" by Donald R. Riley, 1953.

SYMBOLS

The data presented herein are in the form of standard NACA coefficients of forces and moments which are referred to the stability system of axes with the origin coinciding with the intersection of the fuselage center line and the quarter-chord line of the vertical tail. The positive directions of the forces and moments are shown in figure 1. The coefficients and symbols are defined as follows:

C_L	lift coefficient, L/qS_V
C_X	longitudinal-force coefficient, X/qS_V
C_Y	lateral-force coefficient, Y/qS_V
C_l	rolling-moment coefficient, L'/qS_Vb_V
C_m	pitching-moment coefficient, M/qS_Vc
C_n	yawing-moment coefficient, N/qS_Vb_V
L	lift, lb
X	longitudinal force, -drag at $\beta=0°$, lb
Y	lateral force, lb
L'	rolling moment, ft-lb
M	pitching moment, ft-lb
N	yawing moment, ft-lb
q	dynamic pressure, lb/sq ft
b	tail span, ft
c	tail chord, ft
A	aspect ratio
A_e	effective aspect ratio
α	angle of attack of fuselage center line, deg
β	angle of sideslip, deg
S	tail area, sq ft
V	free-stream velocity, ft/sec
E_e	effective edge-velocity correction
C_{L_α}	finite-span lift-curve slope per degree
c_{l_α}	section lift-curve slope per degree
C_{Y_β}	lateral-force derivative, $\partial C_Y/\partial\beta$
C_{l_β}	rolling-moment derivative, $\partial C_l/\partial\beta$
C_{n_β}	yawing-moment derivative, $\partial C_n/\partial\beta$

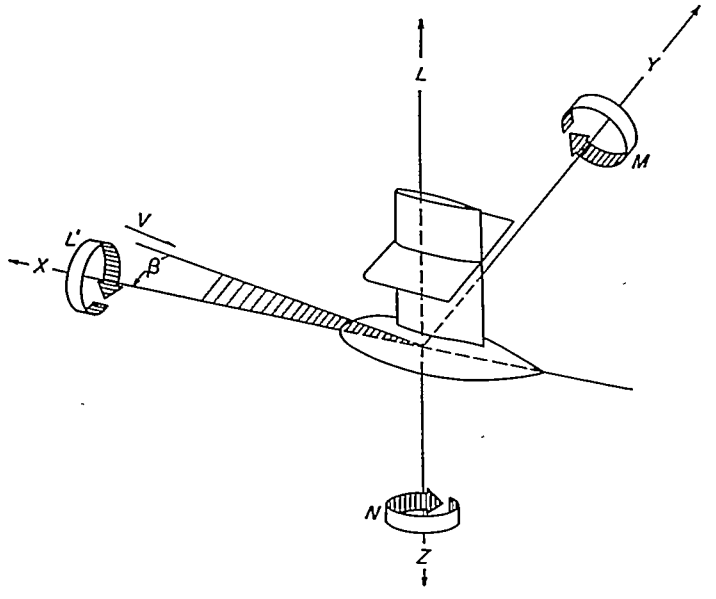

FIGURE 1.—System of axes used. Arrows indicate positive direction of forces and moments.

Subscripts:

V	vertical tail
H	horizontal tail

The symbol C_{l_β} without an additional subscript indicates that the values are for the complete model.

MODELS AND APPARATUS

A vertical-tail model mounted to a stub fuselage was tested alone and in combination with three horizontal tails having spans of 10, 20, and 40 inches in the 6- by 6-foot test section of the Langley stability tunnel. The vertical and horizontal tails were unswept and untapered, having essentially rectangular plan forms with rounded tips and equal chords. The vertical tail was constructed from mahogany and had a span of 20 inches measured from the fuselage center line, an aspect ratio of 2, and an NACA 0012 airfoil section. The horizontal tails were made from $\frac{3}{4}$-inch plywood which was sanded and shellacked to give a smooth surface. Each of the horizontal tails had a rounded leading edge and a sharp trailing edge in order to simulate an airfoil shape in cross section. The fuselage used in the investigation was a body of revolution constructed from mahogany and designed so that the fuselage length was twice that of the vertical-tail chord. Details of the model and the principal dimensions are presented in figure 2. Ordinates for the stub fuselage and vertical-tail airfoil section are listed in table I. Photographs of the composite model showing several of the horizontal-tail sizes and locations are presented in figure 3.

TESTS

Tests were conducted on the stub fuselage with and without the vertical tail and with the vertical tail in combination with each of three horizontal tails located at five different vertical positions relative to the vertical tail. The five vertical locations of the horizontal tails are referred to herein as positions A to E. (See fig. 2.) The model was mounted in the tunnel with the fuselage center line coinciding with the tunnel center line for zero sideslip and zero angle of attack. For each configuration tested, the model was traversed through an angle-of-sideslip range of $\pm 16°$ at an angle of attack of 0°. Data for the complete model were obtained at 2° increments by means of a six-component balance system. Additional tests to obtain the rolling moment of the horizontal tail about its point of attachment were conducted after the vertical tail had been altered to contain a strain gage to which the horizontal tails were attached. Strain-gage readings were recorded at the same angles as the data for the complete model.

All tests were conducted at a dynamic pressure of 24.9 pounds per square foot which corresponds to a Mach number of about 0.131. The Reynolds number, based on the chord of the vertical tail, was approximately 7.7×10^5.

Approximate corrections, which neglected the effect of the stub fuselage and horizontal tails, were applied to the data for the effects of the jet boundaries. No corrections, however, have been applied for the effects of blocking, turbulence, or support-strut interference.

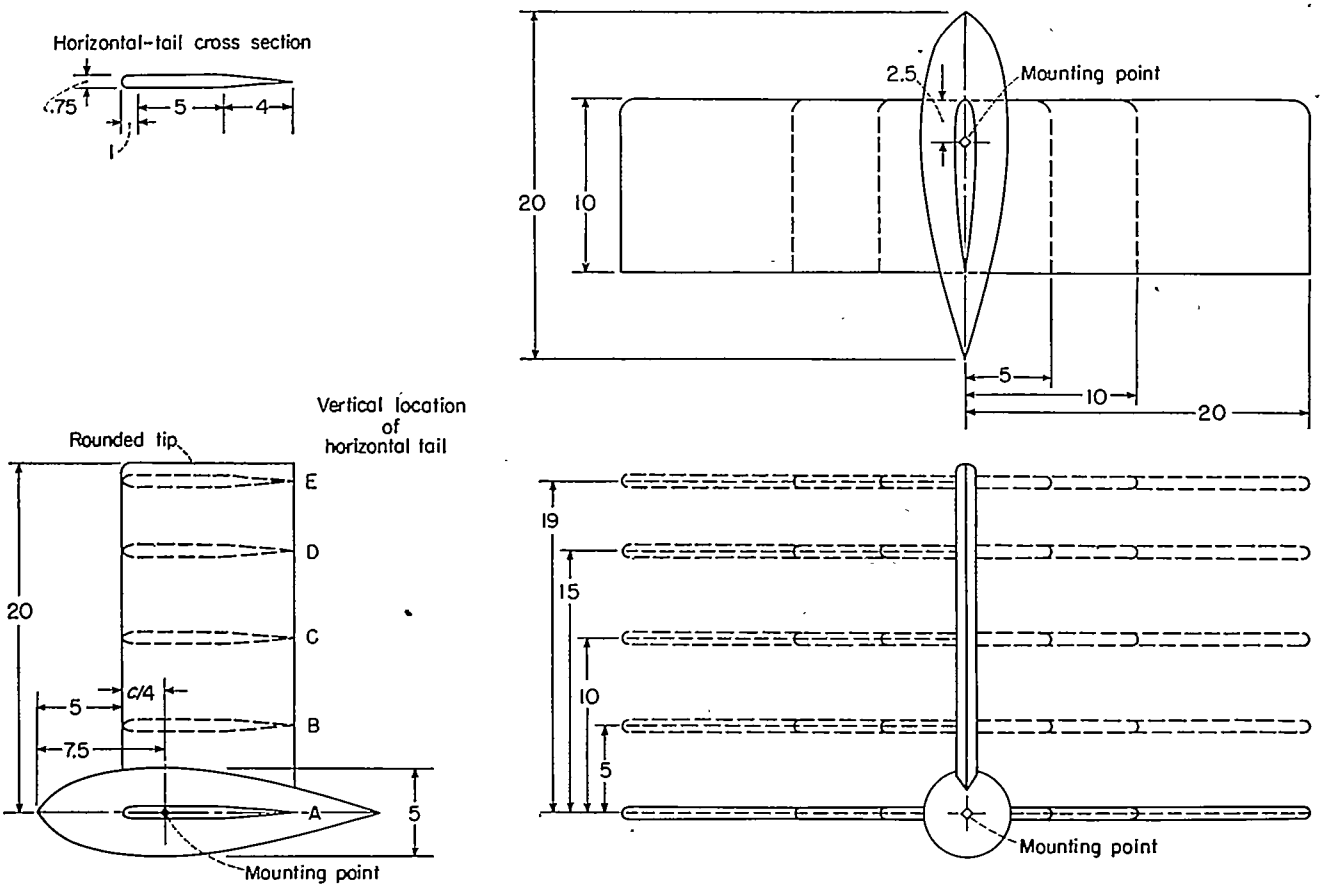

FIGURE 2.—Details of the model showing the horizontal-tail spans and vertical locations of the horizontal tail investigated. (All dimensions are in inches.)

TABLE I.—ORDINATES FOR STUB FUSELAGE AND VERTICAL TAIL

[Airfoil section is symmetrical about the chord and the fuselage is a body of revolution]

Ordinates for stub fuselage

Station, in.	Ordinate, in.
0	0
.50	.70
1.00	1.10
2.00	1.72
3.00	2.03
4.00	2.27
5.00	2.40
6.00	2.48
7.00	2.50
8.00	2.50
9.00	2.47
10.00	2.40
11.00	2.28
12.00	2.10
13.00	1.90
14.00	1.68
15.00	1.40
16.00	1.15
17.00	.85
18.00	.56
19.00	.28
20.00	0

Ordinates for vertical-tail airfoil section (NACA 0012)

Station, in.	Ordinate, in.
0	0
.125	.189
.250	.262
.500	.356
.750	.420
1.000	.468
1.500	.534
2.000	.574
2.500	.594
3.000	.600
4.000	.580
5.000	.529
6.000	.456
7.000	.366
8.000	.262
9.000	.145
9.500	.081
10.000	.013
10.000	0
Leading-edge radius, 0.158	

THEORY

The finite-step method used herein to evaluate subsonic span loadings for the vertical-tail and horizontal-tail combinations in sideslip has been employed by a number of investigators in calculating the loadings on wings of unusual plan form. For example, in reference 5 this method is incident to a determination of the aeroelastic loading on wings. As used herein, the finite-step method consists of replacing the tail surfaces by a finite number of horseshoe vortices which are distributed across both the vertical- and the horizontal-tail spans with the bound portion located at the quarter-chord line. The velocity normal to the surface, resulting from the complete vortex system, is then calculated at the three-quarter-chord line for the midspan station of each horseshoe vortex. At these control points, the boundary condition of tangential flow is applied. The boundary condition is satisfied by equating the normal velocity resulting from the vortex system to the component of the free stream normal to the surface. For the vertical tail the free-stream component is $V\beta$ and for the horizontal it is $V\alpha$, which is zero since α was held zero for the experimental tests. The angles α and β, of course, are expressed in radians. The expression for the normal velocity at a given control point contains the unknown circulations of all horseshoe vortices used to define the configuration. When the expressions for all the control points are solved simultaneously, values of the unknown circulations and, hence, the span loadings are obtained. The important concept of the quarter-chord and three-quarter-chord lines to obtain the angle of attack of a surface was first advanced by Pistolesi and is discussed by Weissinger in reference 6.

The expressions used to calculate the sidewash and downwash at any point in space due to a single horseshoe vortex

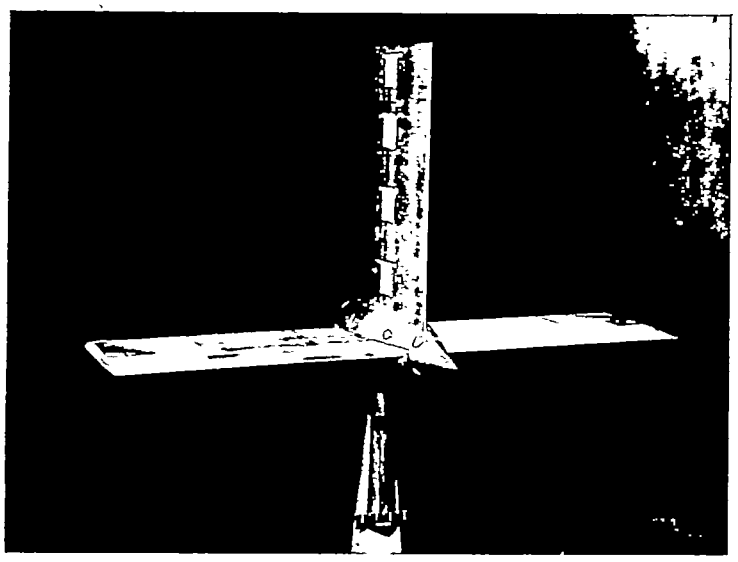

(a) 40-inch horizontal tail at location A.

FIGURE 3.—Three-quarter views of the stub-fuselage and vertical-tail model with the three horizontal tails investigated mounted in the 6- by 6-foot test section of the Langley stability tunnel.

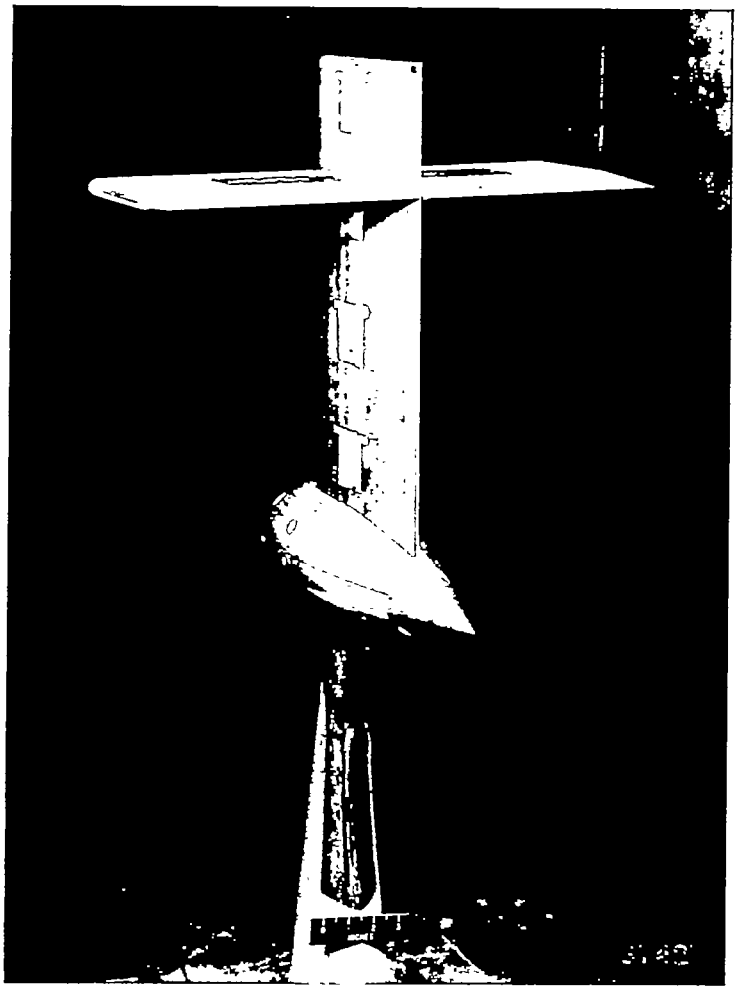

(b) 20-inch horizontal tail at location D.

FIGURE 3.—Continued.

were obtained from reference 7. These expressions show that the desired velocity components are proportional to the product of the circulation and some function of the geometry. Tabulated values of the geometric contribution in terms of the vortex semispan are presented in references 8 and 9 for the downwash where the control point is located in the same

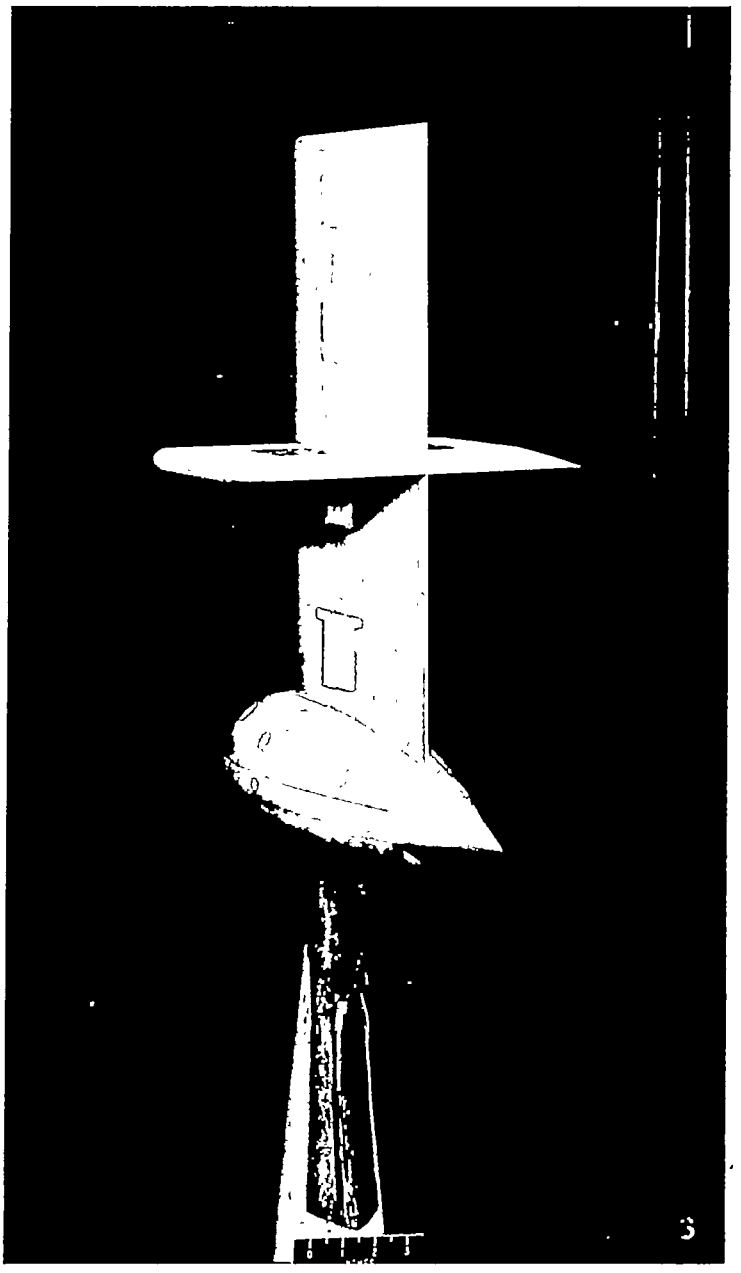

(c) 10-inch horizontal tail at location C.

FIGURE 3.—Concluded.

plane as the horseshoe vortex. All sidewash values were found from the sidewash expressions given in reference 7 because no sidewash tables were available.

A correction for the difference between the actual and the theoretical values of the section lift-curve slope must be applied to the calculated results since the finite-step method is based on the theoretical thin-airfoil-section lift-curve slope of $2\pi/57.3$. For the case where the actual section lift-curve slope c_{l_α} is about constant across the span and where only a small correction is needed, it is sufficient to reduce the values by the ratio $\frac{57.3c_{l_\alpha}}{2\pi}$. For more exacting computations, the position of the control point may be shifted to account for variations in c_{l_α}. (See ref. 10.)

Calculations of the span loadings which were reduced to force and moment derivatives were performed with four horseshoe vortices distributed across the quarter-chord line of the vertical tail from the fuselage center line to the tip so

that each horseshoe vortex had a span of 5 inches. Using this vortex span resulted in an even distribution of horseshoe vortices across each of the three horizontal tails. The choice of four vortices to represent the vertical tail was obtained from a short analysis, given in appendix A, of the effect of the number of horseshoe vortices. Sketches of several of the vortex configurations calculated, showing variations in span and location of the horizontal tail, are presented in figure 4. The number of equations necessary to solve for each different configuration could be reduced since the loadings on the two panels of the horizontal tail were of equal magnitude but opposite in sign. For the configuration involving the 40-inch horizontal tail, for example, the calculations involved a solution of only eight simultaneous equations. The solution of eight equations by use of the Crout method in conjunction with manually operated computing machines required about 5½ hours. Using a relay-type computer reduced the time required to about 3 hours.

Several additional calculations for comparison purposes were performed for the vertical tail in combination with the 10-inch horizontal tail by using eight horseshoe vortices distributed across the vertical tail instead of four.

RESULTS AND DISCUSSION

PRESENTATION OF RESULTS

The experimental results for the fuselage alone, with the vertical tail, and with the vertical tail in combination with each of the three horizontal tails at various vertical locations are presented in figures 5 and 6. In addition, the measurements obtained for the rolling moment of the horizontal tail about its point of attachment to the vertical tail are presented in figure 7. Experimental values for the static-lateral-stability derivatives C_{Y_β}, C_{l_β}, and $C_{l_{\beta_H}}$ showing the effects of span and vertical location of the horizontal tail are summarized in figures 8 and 9. A short analysis of the effect of the number of horseshoe vortices employed is presented in appendix A and some approximate calculated effects of the stub fuselage are discussed in appendix B. A summary of the calculated results for the combinations of vertical and horizontal tails without a fuselage is presented in figure 10 and a comparison of experimental and calculated results (including fuselage effect) is shown in figures 11 and 12.

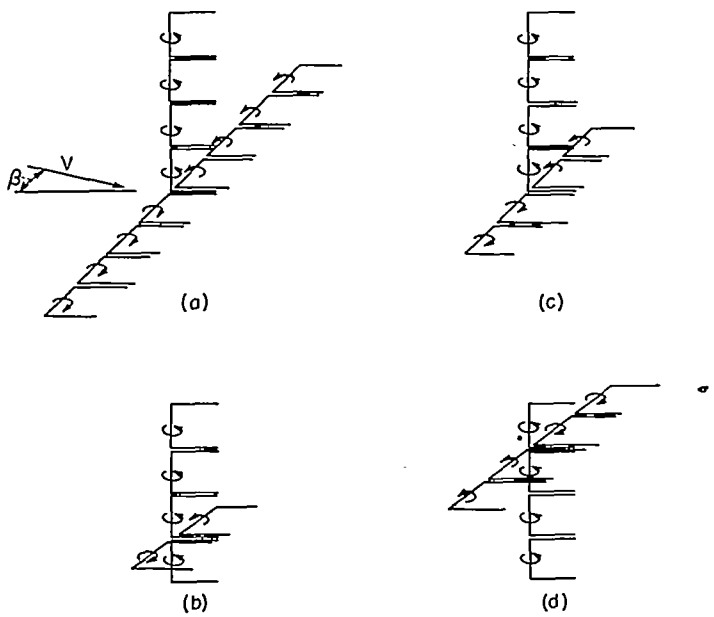

(a) 40-inch horizontal tail at position A.
(b) 10-inch horizontal tail at position B.
(c) 20-inch horizontal tail at position A.
(d) 20-inch horizontal tail at position D.

FIGURE 4.—Sketches of several vortex representations of tail configurations calculated in the absence of a fuselage. Direction of rotation of each horseshoe vortex is indicated for positive circulation. Gaps between adjacent trailing vortices are shown to indicate the number of horseshoe vortices used. All calculations were performed with adjacent trailing vortices coinciding and extending to infinity.

BASIC DATA

Experimental results for the stub fuselage alone and with the vertical tail are presented in figure 5. The fuselage-alone data indicate a slightly negative C_{Y_β} and a C_{n_β} of zero. Theoretical considerations of the fuselage alone indicate a slight instability for C_{n_β}; however, the magnitude of the values of C_n expected for this fuselage is not within the accuracy of the balance system used. The C_{n_β} obtained for the fuselage—vertical-tail combination is probably due to the C_{n_β} of the vertical tail alone and possibly to a small increment due to interference effects. Although the force and moment center for the tests was located at the quarter-chord line of the vertical tail, both theoretical and experimental results for wings show a forward shift in the aerodynamic center with decreasing aspect ratio.

The horizontal-tail-on data (fig. 6) indicate noticeable variations in C_{Y_β} and C_{l_β} for changes in horizontal-tail span and vertical locations. These results are summarized in figures 8 and 9 and are discussed in the following sections. The pitching moment C_m shows an increase in value for an increase in span at all locations except A and for a given span as the tail location is shifted from A to E. Most of the increase indicated can be attributed to changes in the longitudinal force for the various horizontal tails and to the vertical location of those forces. The effect on C_X of increasing the span is clearly indicated at $\beta=0$ and, at the higher angles of sideslip, the end-plate effect of the horizontal tails is evident at locations A and E. Little change is apparent in C_{n_β} for the horizontal tail-on and tail-off configurations. Some variation in C_L occurs for all angles of sideslip and is probably the combined result of several factors, among them being support interference, some fuselage effect on the horizontal tails, especially at the lower positions, and possibly a slight misalinement of the horizontal surfaces relative to the free stream. The variations do not appear to be too significant except for location A where a blanketing of the inboard portion of the trailing semispan is produced by the fuselage.

The strain-gage measurements for the horizontal-tail rolling moments (fig. 7) show a slight differential angle of attack between the two horizontal-tail panels, especially for the 40-inch tail span. This difference, however, is not too important since the primary concern is $C_{l_{\beta_H}}$ and these curves appear linear over a sideslip range of at least $\pm 8°$. Particular care was taken in conducting these tests to eliminate horizontal-tail dihedral. The experimental results for $C_{l_{\beta_H}}$ are summarized in figures 8 and 9 which are discussed subsequently.

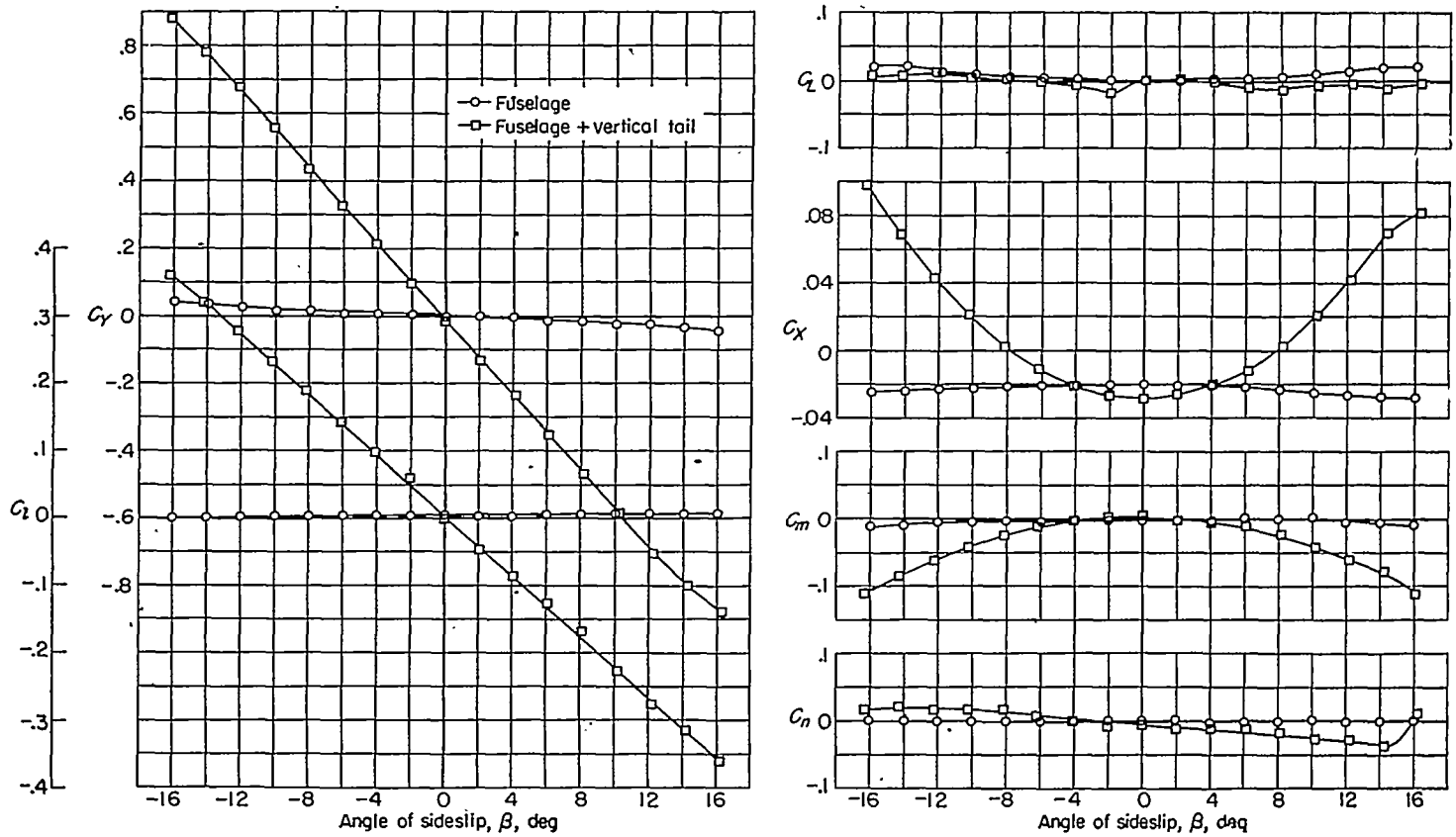

FIGURE 5.—Experimental aerodynamic characteristics of the stub fuselage with and without the vertical tail attached.

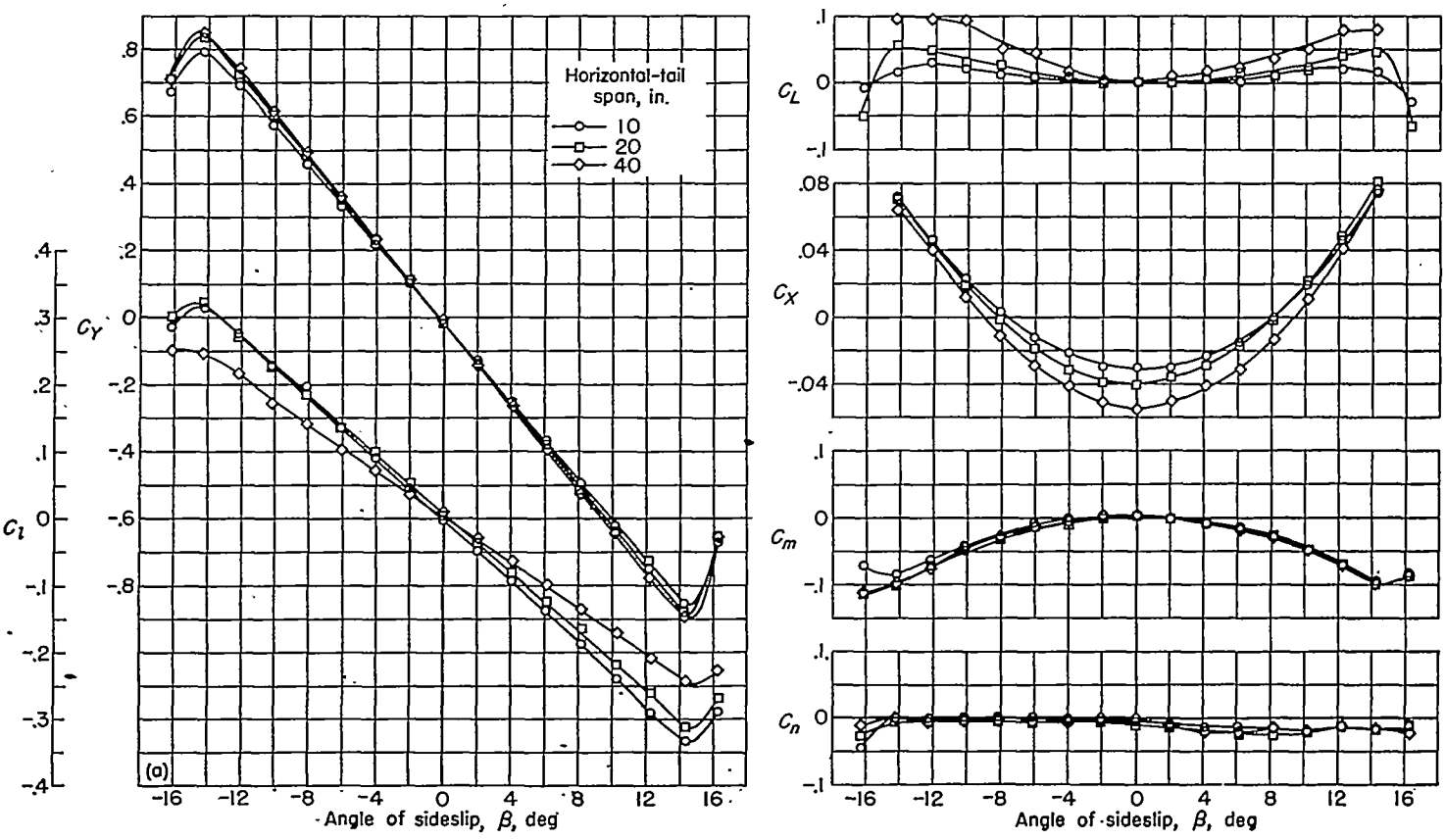

(a) Horizontal tails at location A.

FIGURE 6.—Experimental aerodynamic characteristics of the unswept tail assembly, having horizontal tails of 10-, 20-, and 40-inch spans, for the various vertical locations of the horizontal tail relative to the vertical tail.

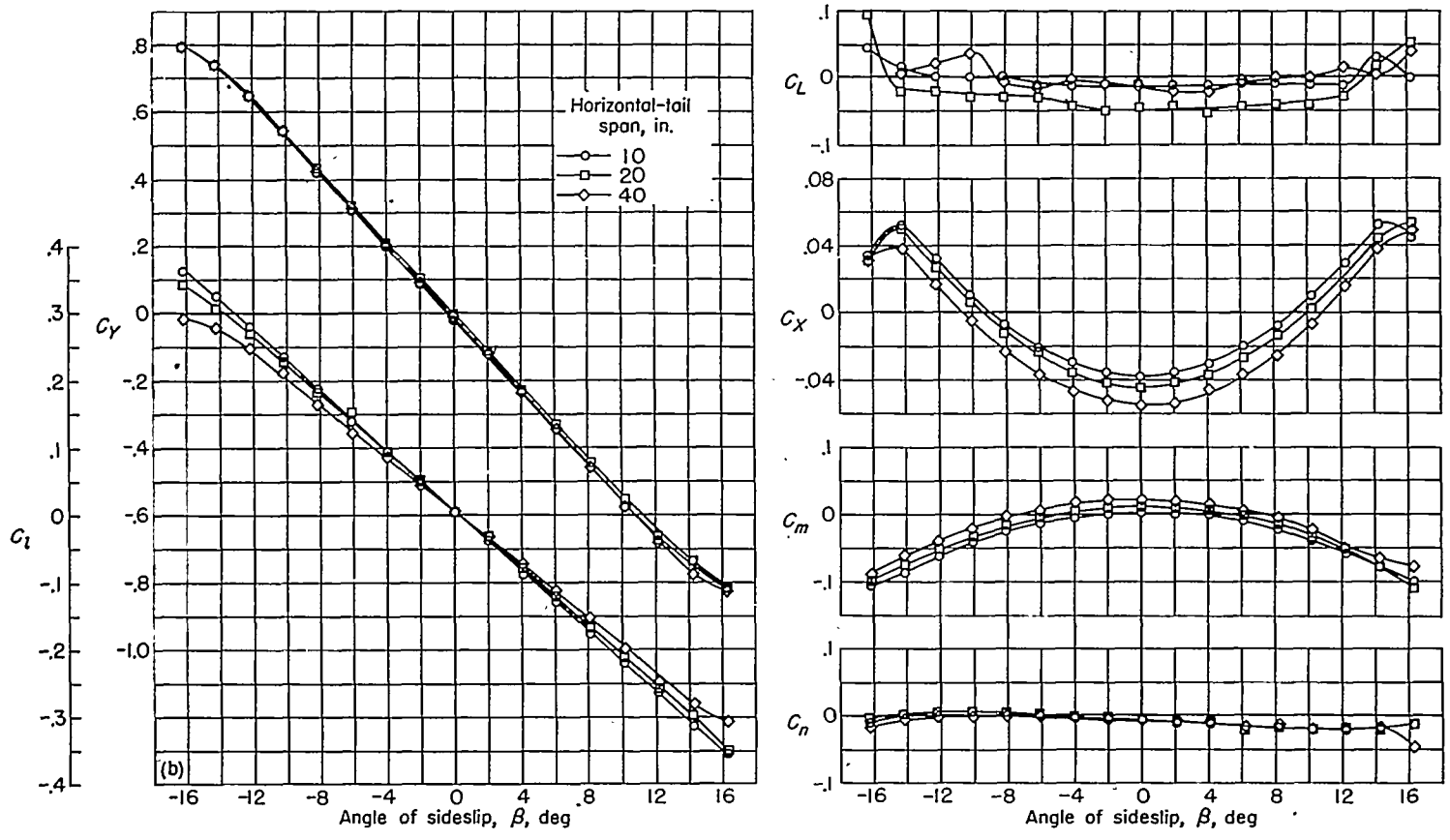

(b) Horizontal tails at location B.

FIGURE 6.—Continued.

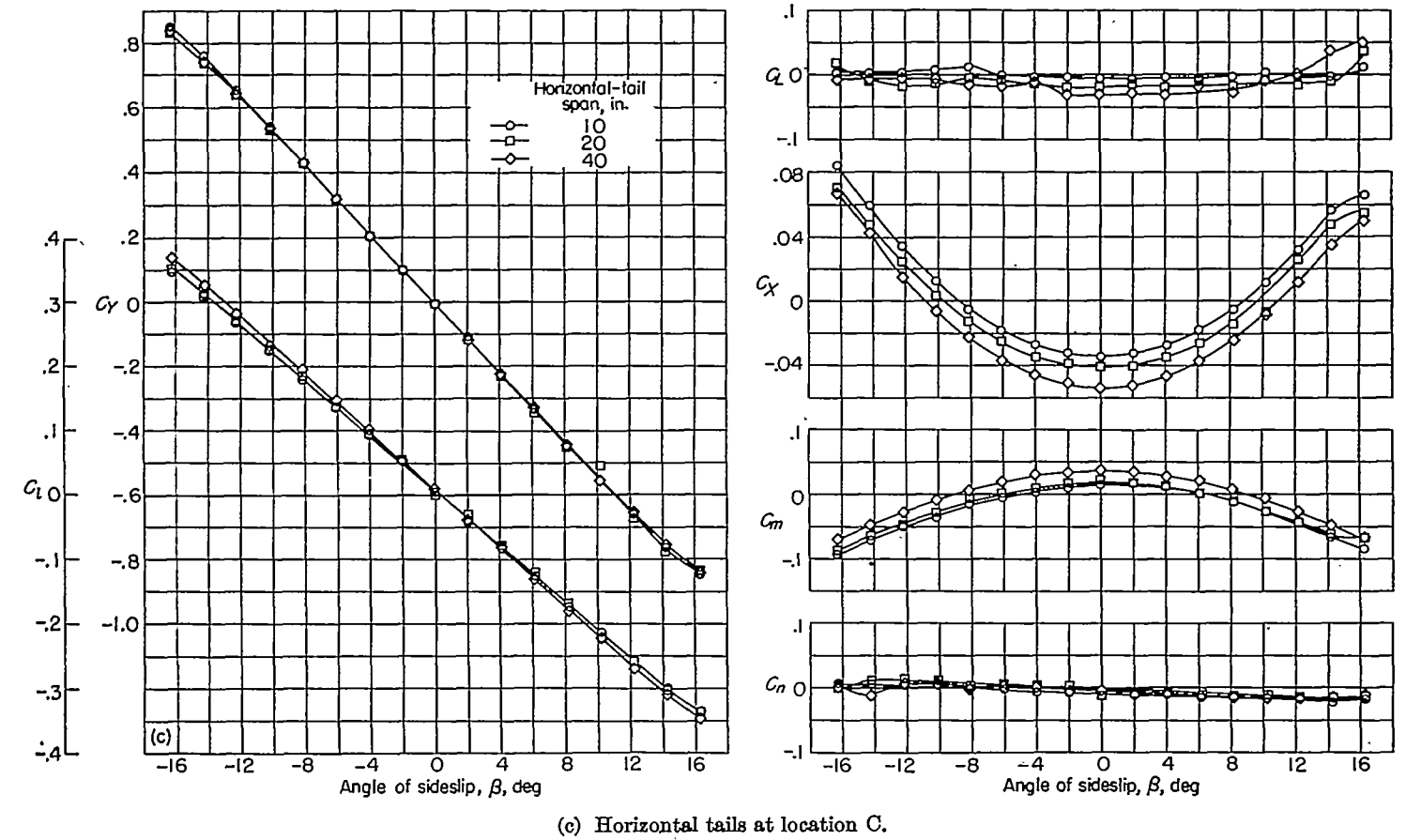

(c) Horizontal tails at location C.

FIGURE 6.—Continued.

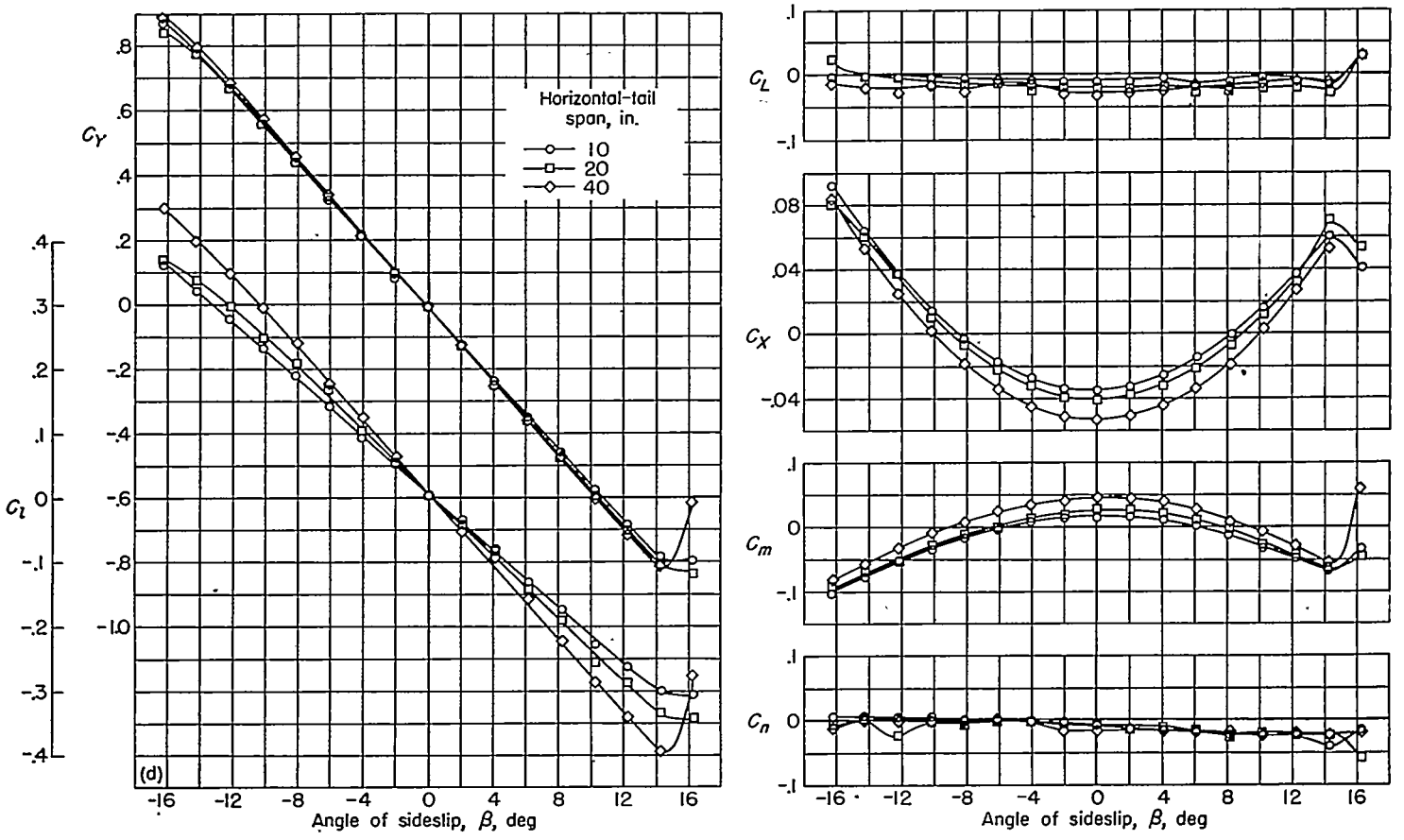

(d) Horizontal tails at location D.

FIGURE 6.—Continued.

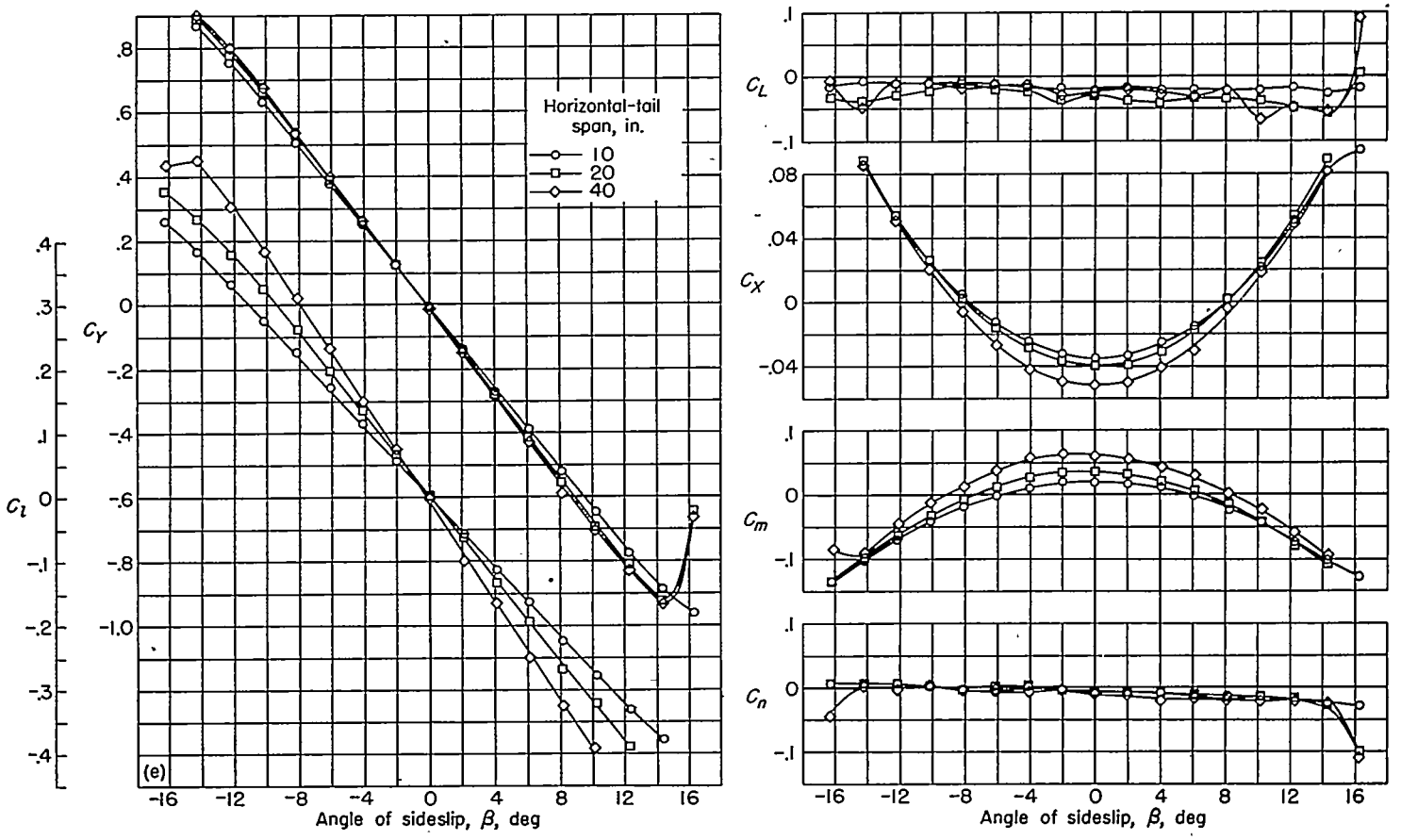

(e) Horizontal tails at location E.

FIGURE 6.—Concluded.

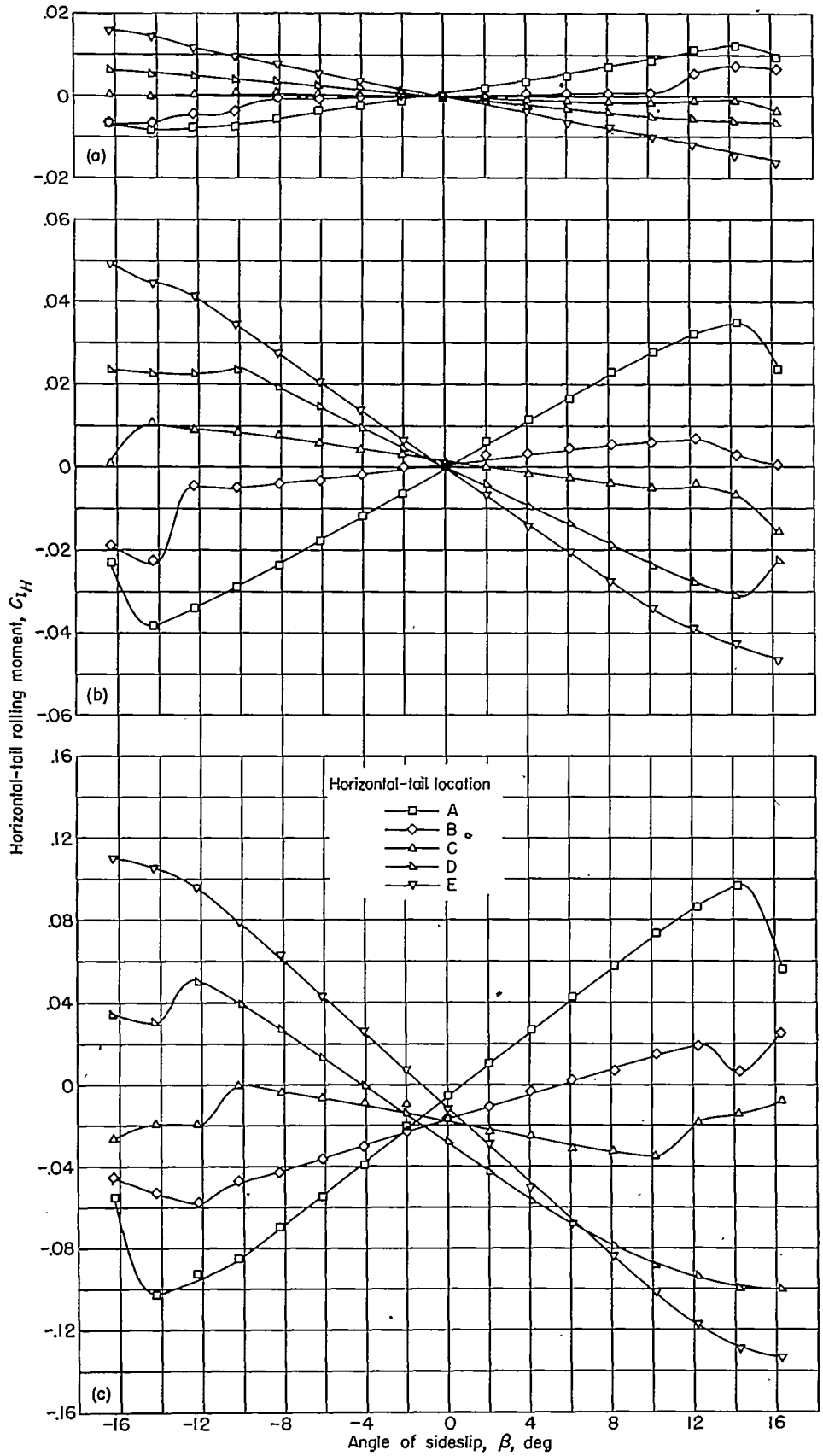

(a) 10-inch horizontal-tail span.
(b) 20-inch horizontal-tail span.
(c) 40-inch horizontal-tail span.

FIGURE 7.—Strain-gage measurements for the rolling moment of the 10-, 20-, and 40-inch horizontal tails about their points of attachment to the vertical tail for the five different vertical locations investigated.

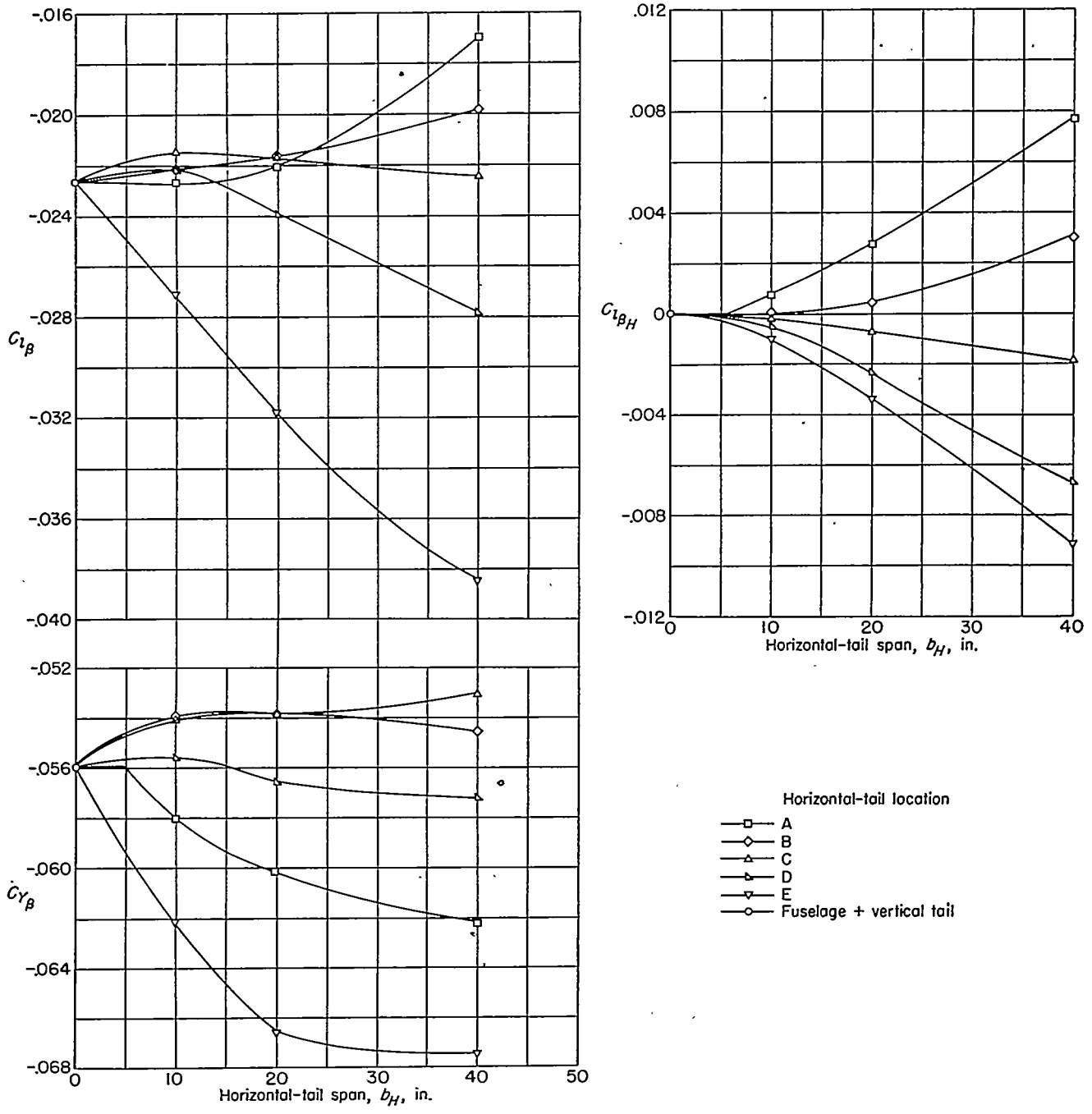

FIGURE 8.—Effect of horizontal-tail span on the experimental results for the lateral-force derivative C_{Y_β}, the rolling-moment derivative of the complete tail assembly C_{l_β}, and the rolling-moment derivative of the horizontal tail $C_{l_{\beta_H}}$.

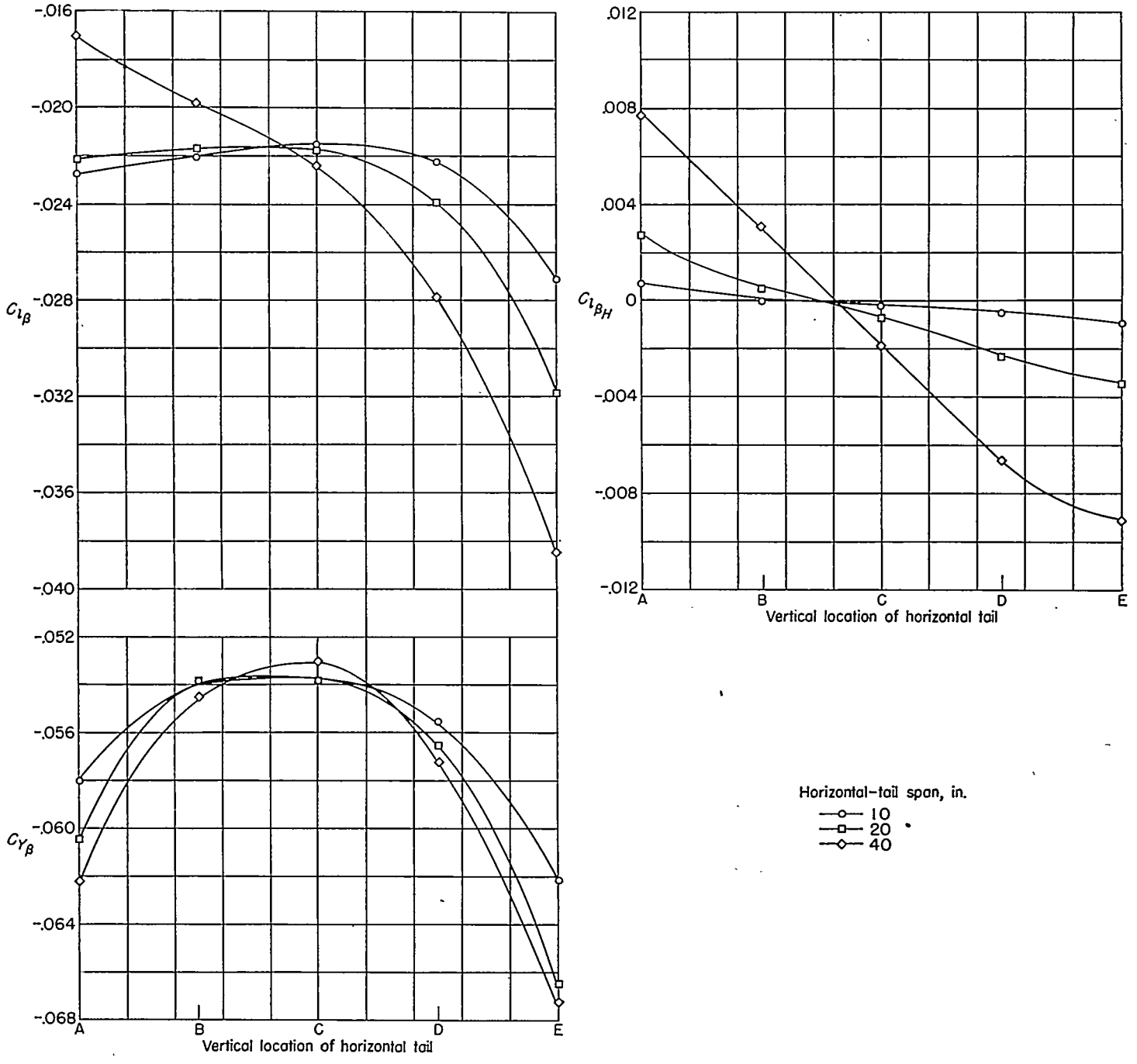

FIGURE 9.—Effect of vertical location of the horizontal tail on the experimental results for the lateral-force derivative C_{Y_β}, the rolling-moment derivative of the complete tail assembly C_{l_β}, and the rolling-moment derivative of the horizontal tail $C_{l_{\beta_H}}$.

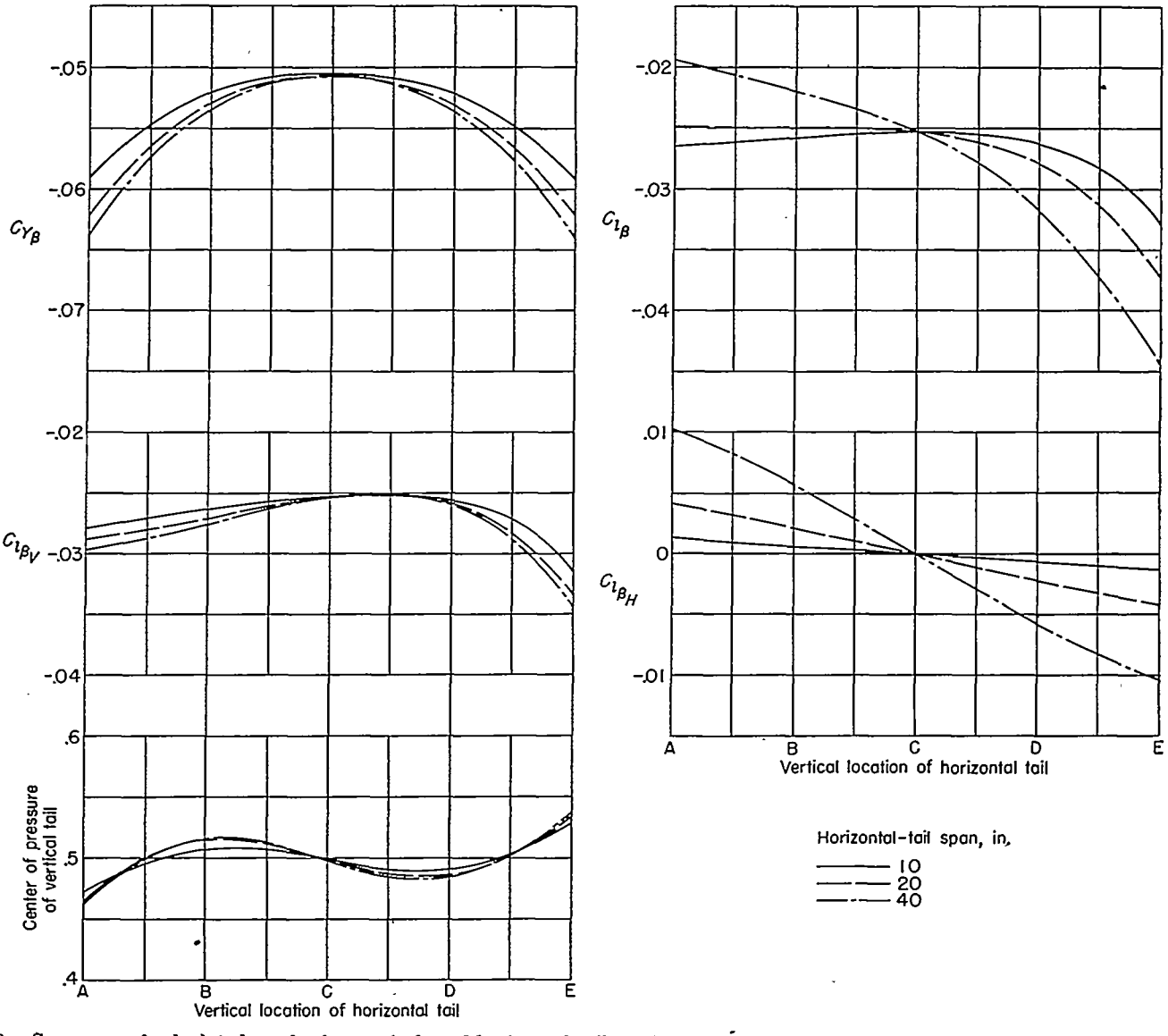

FIGURE 10.—Summary of calculated results for vertical- and horizontal-tail combinations investigated for no fuselage present. Results are based on c_{l_α} of $2\pi/57.3$.

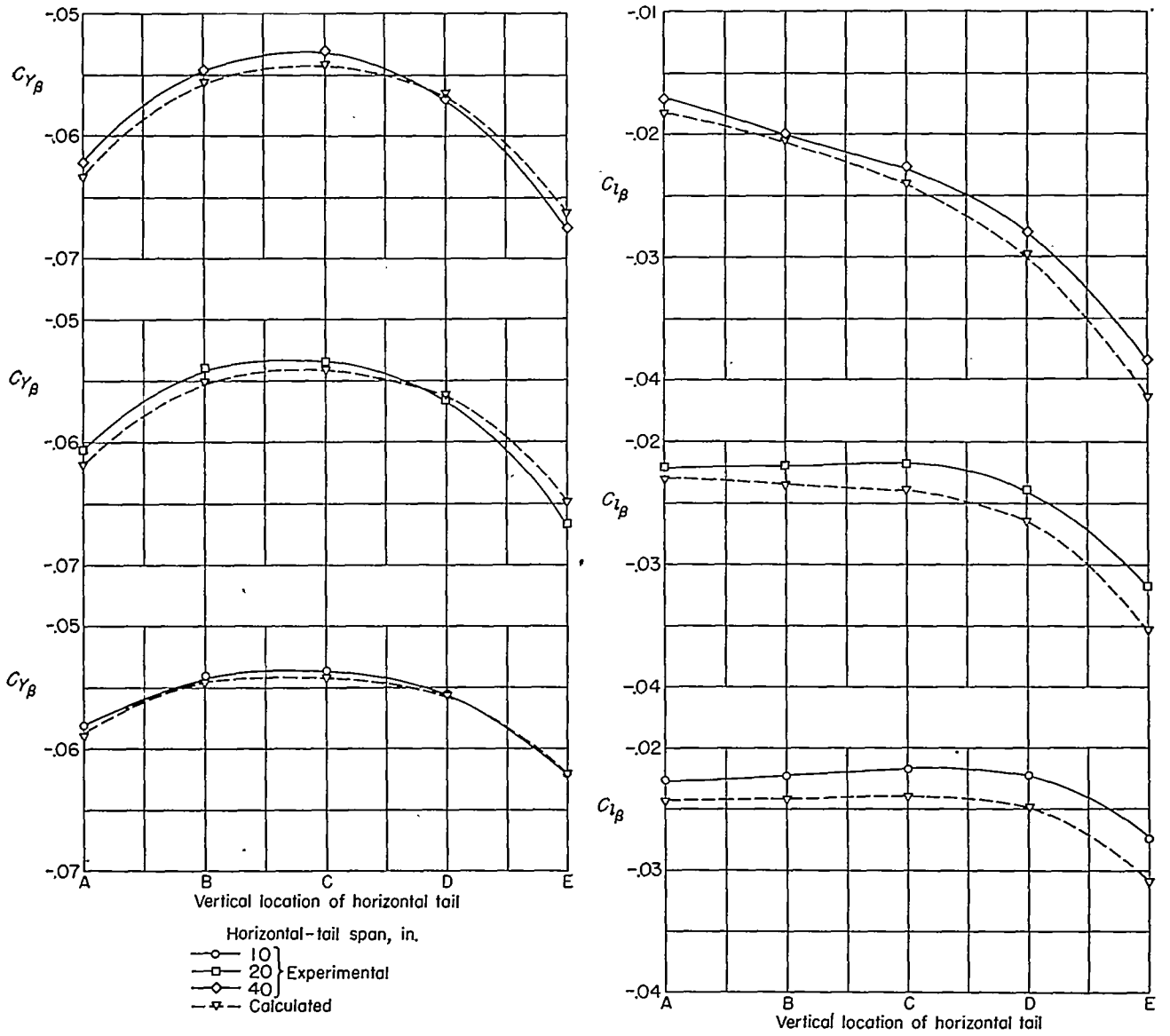

FIGURE 11.—Comparison of experimental and calculated results for the lateral-force derivative C_{Y_β} and the rolling-moment derivative for the complete tail assembly C_{l_β}. Calculated results include an estimation of the fuselage effect and are corrected for the effect of section lift-curve slope.

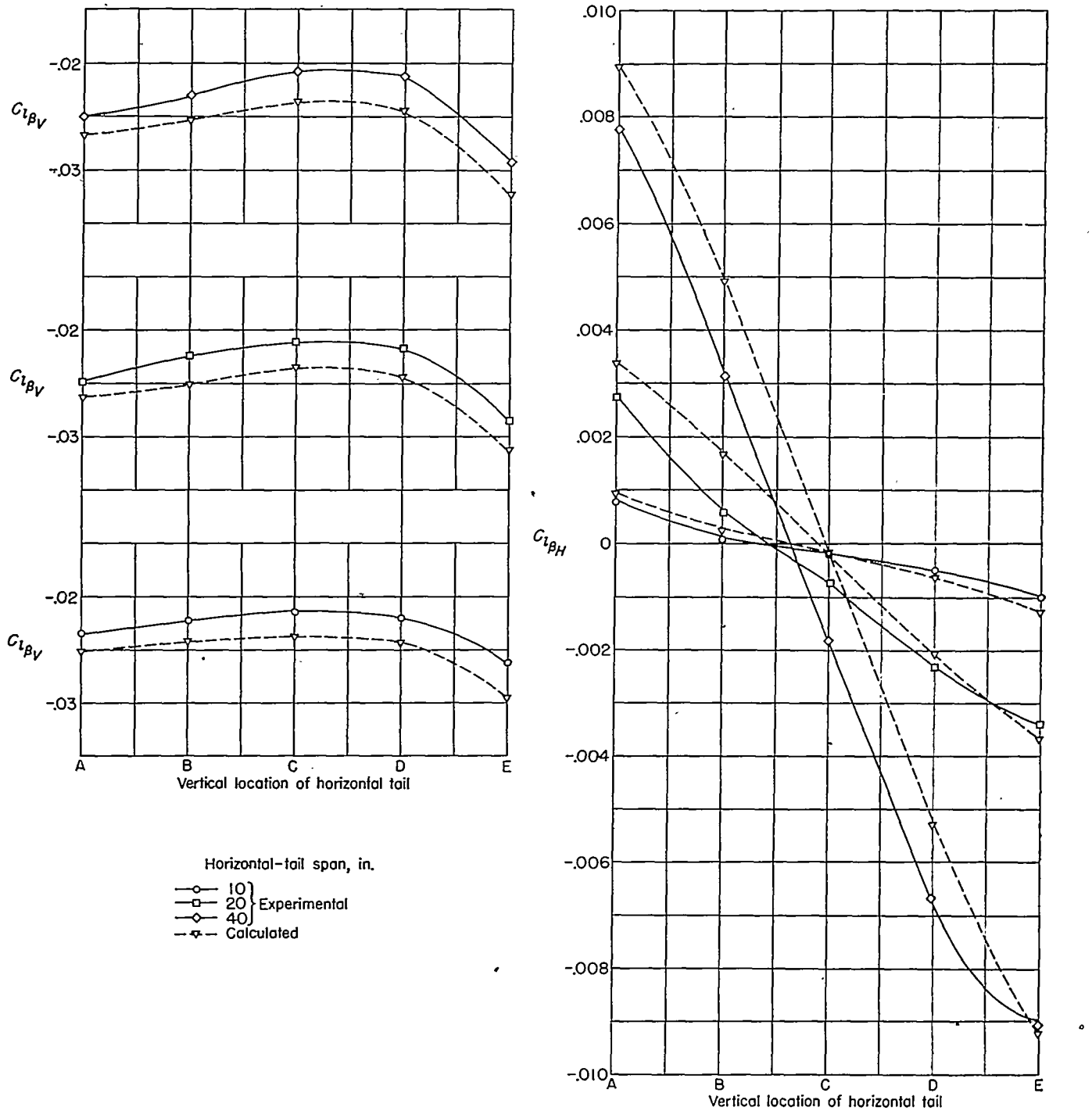

FIGURE 12.—Comparison of experimental and calculated results for the rolling-moment derivative of the horizontal tail $C_{l_{\beta_H}}$ and the rolling-moment derivative of the vertical-tail—stub-fuselage combination $C_{l_{\beta_V}}$. Calculated results include an estimation of the fuselage effect and are corrected for the effect of section lift-curve slope.

EFFECT OF SPAN ON STABILITY DERIVATIVES

The experimental results for the static-lateral-stability derivatives C_{Y_β}, C_{l_β}, and $C_{l_{\beta_H}}$ are presented in figure 8 as functions of horizontal-tail span. The data indicate that the greatest influence of span on C_{Y_β} was obtained when the horizontal tails were located at either tip of the vertical tail (locations A and E). At location E the end-plate effect of the horizontal tail provided relatively large increases in the magnitude of C_{Y_β} for corresponding increases in span as long as the horizontal-tail span did not exceed the span of the vertical tail (20 inches). Increasing the span above this value provided only small additional increases in the magnitude of C_{Y_β}. For example, increasing the span from 20 to 40 inches provided an additional increase of less than 2 percent in the magnitude of C_{Y_β}. The C_{Y_β} curve for location A exhibits the same general trend as the curve for location E and at somewhat larger tail spans an increase in span probably results in even smaller increases in C_{Y_β} than the present range of tail sizes indicates. Although horizontal-tail span apparently has little effect at tail locations B and C, except possibly for the smaller tail spans, figure 8 does show that the use of these locations can result in a slightly more positive C_{Y_β} than for the vertical-tail—fuselage combination. Of particular interest is the fairing of the curve of C_{Y_β} for location A in the region of b_H of 5 inches. The constant-value line shown is intended to convey that almost all of the horizontal tail is contained within the fuselage for the range of b_H values from 0 to approximately 5 inches, and, thus, the fuselage—vertical-tail configuration applies at every point in this region. The constant value of the vertical-tail—fuselage combination for the region of b_H from 0 to about 5 inches is indicated not only for C_{Y_β} but also for the rolling derivatives C_{l_β} and $C_{l_{\beta_H}}$. Thickness of the vertical tail also provides a similar effect; however, it was neglected in the plotting of the curves.

The effect of horizontal-tail span on the rolling-moment derivative of the horizontal tail $C_{l_{\beta_H}}$ is evident at all horizontal-tail locations and appears to become increasingly more important as the horizontal tails are moved closer to the tips of the vertical tail and as the horizontal-tail span increases. The effect under the latter condition can be attributed mainly to the increased distance from the loading to the axis of roll. A comparison of the values of C_{l_β} and $C_{l_{\beta_H}}$ indicates that the magnitude of $C_{l_{\beta_H}}$ for the larger tail spans can provide a large contribution to the value of the rolling-moment derivative of the complete tail assembly. An indication of the magnitude of the $C_{l_{\beta_H}}$ contribution can be seen by noting, for example, that the 40-inch tail at locations A and E produces a rolling moment of about 35 to 40 percent of the rolling moment of the fuselage—vertical-tail combination. The unsymmetrical appearance of the $C_{l_{\beta_H}}$ data for corresponding spans relative to $C_{l_{\beta_H}}=0$ for tail locations B and D can be attributed to the influence of the stub fuselage. A direct indication of the magnitude of the fuselage interference can be obtained at location C since the absence of a fuselage would result in a value of $C_{l_{\beta_H}}$ of zero for all horizontal-tail spans. The effect of horizontal-tail span on C_{l_β} shows a very strong influence at location E. For spans less than the vertical-tail span (20 inches), the dominating effect at location E appears to be the additional vertical-tail loading and associated center-of-pressure shift produced by the end-plate effect. For horizontal-tail spans above 20 inches, however, the rapid rate of change of C_{l_β} with span is mainly the effect of $C_{l_{\beta_H}}$. At location D, the principal effect of span on C_{l_β} can also be traced to the $C_{l_{\beta_H}}$ contribution, as can the variation appearing for locations A and B for b_H values above 20 inches. For values of b_H less than 20 inches, the interaction of the rolling-moment derivative of the vertical tail and $C_{l_{\beta_H}}$ provides only minor span effects at locations A, B, and C.

EFFECT OF LOCATION ON STABILITY DERIVATIVES

The experimental lateral-stability derivatives C_{Y_β}, C_{l_β}, and $C_{l_{\beta_H}}$ are presented in figure 9 as functions of vertical location of the horizontal tail. Horizontal-tail location appears to influence C_{Y_β} irrespective of horizontal-tail span, the greatest variation occurring for horizontal-tail locations near either extremity of the vertical tail. On $C_{l_{\beta_H}}$, changes in vertical location are of particular importance since the values change in sign. For tail locations near the base of the vertical tail (A and B), the rolling moment of the horizontal tail resists the rolling moment of the vertical tail but, at locations C, D, and E, the horizontal-tail rolling moment is additive to the rolling moment of the vertical tail. At location C, the magnitude of $C_{l_{\beta_H}}$ for various spans gives a direct indication of the fuselage interference at this location. The greatest change in C_{l_β} occurs for the 40-inch span over the complete range of locations. For horizontal-tail spans of 10 and 20 inches, the greatest variation in C_{l_β} occurs for tail locations near position E.

The experimental data are presented in figure 9 for the tail located at the tip of the vertical tail and, although the model tested had the horizontal tail mounted slightly below the tip, the thickness of the horizontal tail was such that the vertical tail extended only slightly above the horizontal tail. (See fig. 2.) The unsymmetrical appearance of the data, particularly noticeable for C_{Y_β} and $C_{l_{\beta_H}}$, can be traced to the addition of the fuselage to the vertical- and horizontal-tail combinations. In order to magnify the experimental

results, scales were chosen for the stability derivatives in figures 8 and 9 which, in general, are not justified by the experimental accuracy. In addition, it should be remembered that all the stability derivatives presented herein were obtained by using coefficients based on the vertical-tail area.

COMPARISON OF CALCULATED AND EXPERIMENTAL RESULTS

Spanwise step loadings for each of the combinations of vertical and horizontal tails tested were calculated as outlined in the section entitled "Theory." These loadings expressed in terms of the static-lateral-stability derivatives C_{Y_β}, C_{l_β}, $C_{l_{\beta_H}}$, and $C_{l_{\beta_V}}$ and based on a c_{l_α} of $2\pi/57.3$ are presented in figure 10. Although these results are not directly comparable with the experimental data since the fuselage was omitted in the calculations, they do represent a theoretical solution for the intersecting surfaces.

To the values in figure 10 have been applied a correction for the effect of section-lift-curve slope and a correction, as discussed in appendix B, accounting for the effect of the fuselage. The section-lift-curve-slope correction consisted of reducing the values of the stability derivatives in proportion to the ratio $\frac{57.3c_{l_\alpha}}{2\pi}$. Airfoil-section data of reference 11 indicate that the c_{l_α} for an NACA 0012 airfoil section has a value about 10 percent less than the theoretical; unpublished results obtained for some wings by the finite-step method employing 10 or 20 discrete horseshoe vortices show that variations in c_{l_α} of this magnitude or less provide only minor changes in the span-load distribution as compared with the stricter solution involving a relocation of the control point at a position other than the three-quarter-chord point. The c_{l_α} of the horizontal tail was assumed to be equal to the c_{l_α} of the vertical tail; this assumption, although not strictly correct, would appear to be a reasonable estimate of the c_{l_α} of the horizontal tail. The results of figure 10, corrected for section-lift-curve slope and including an estimation of the fuselage effect, are presented in figures 11 and 12 and compared with corresponding experimental data. The results are presented as a function of location in order that the calculated values for the 10-inch horizontal-tail combinations, which have the most accurate estimation of the fuselage effect, can be directly compared with experimental data. The comparison in figure 11 shows excellent agreement for C_{Y_β} at all spans. Good agreement was also obtained for C_{l_β}, the largest variation between experimental and calculated results occurring for the 10-inch horizontal-tail-on configuration.

In figure 12, the C_{l_β} of the complete model has been broken down into its component parts, $C_{l_{\beta_H}}$ and $C_{l_{\beta_V}}$; the fuselage is included in $C_{l_{\beta_V}}$. The results appear to be in good agreement with experimental values. Increasing the number of horseshoe vortices defining the configurations and using a better estimation of the fuselage effect would probably result in a much better agreement for C_{l_β} and $C_{l_{\beta_V}}$. The use of only four horseshoe vortices results in a spanwise step loading giving only an approximate vertical location of the center of pressure of the vertical tail which should be responsible for part of the variation present. The calculations for $C_{l_{\beta_H}}$ for the 10-inch horizontal-tail-on configurations are in excellent agreement with experimental values. Using a similar method for estimating the fuselage effect for the 20- and 40-inch tail configurations would seem to provide as good agreement as for the 10-inch tail configuration. (See appendix B.) Although these improvements in the calculations are apparent, the amount of time required for computing the loadings was not felt to be justified in view of the good agreement obtained thus far. The results definitely show that a good estimation of the static-stability derivative can be obtained for intersecting surfaces by use of the finite-step method. Utilizing this method in conjunction with relay-type computing machines should provide a simple means for investigating the effects of variations in plan form, taper ratio, and sweep on the span loadings of intersecting surfaces.

EFFECTIVE ASPECT RATIO

Using the variation of lift-curve slope with aspect ratio for four horseshoe vortices distributed across the span of a rectangular-plan-form wing, which is part of the results of a short analysis on the effect of the number of horseshoe vortices on C_{L_α} as presented in appendix A, in conjunction with C_{Y_β} from figure 10, makes it possible to obtain the end-plate effect of the horizontal tail in terms of the ratio A_e/A. Expressing the effect of the horizontal tail in this manner makes comparison of the calculated results with the synthesized results of reference 3 possible. The comparison expressing A_e/A as a function of horizontal-tail location is presented in figure 13 and indicates a noticeable effect of horizontal-tail span for the calculated results obtained herein. The results of reference 3 which are indicated in the figure by the dashed line apply for all horizontal-tail spans. A small variation of A_e/A with span was obtained in reference 3; however, it was considered negligible. As shown in figure 14, in which the computations for four and eight horseshoe vortices distributed across the vertical tail for the 10-inch horizontal-tail configurations are presented, a large part of the effect of span may possibly be the result of the number of horseshoe vortices employed. Figure 14 appears to indicate that, although the variation in A_e/A due to span may possibly be reduced by increasing the number of horseshoe vortices defining the configuration, the values of A_e/A

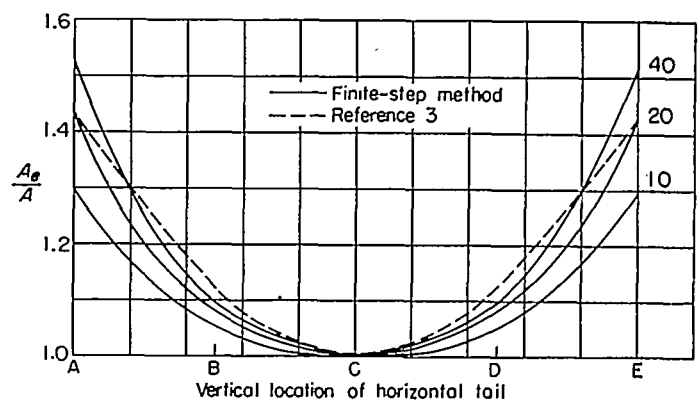

FIGURE 13.—Calculated values of A_e/A for the vertical tail by the finite-step method as a function of horizontal-tail location for various horizontal-tail spans compared with the synthesized results of reference 3.

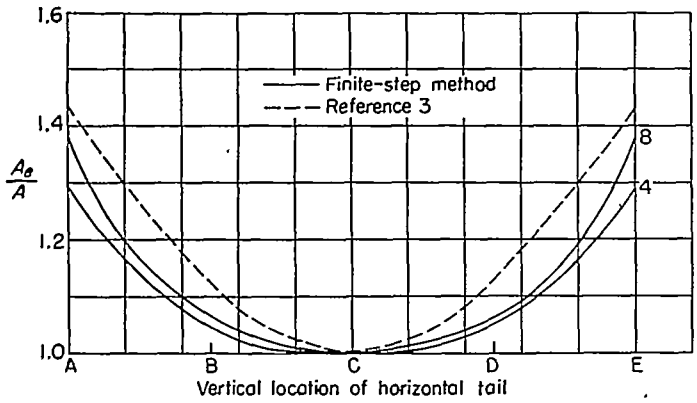

FIGURE 14.—Values of A_e/A for the vertical tail determined by the finite-step method as a function of horizontal-tail location for 10-inch horizontal tails only, using four and eight horseshoe vortices across the vertical-tail span (with one and two horseshoe vortices, respectively, on each panel of the horizontal tail), compared with the synthesized results of reference 3.

predicted by the finite-step method would be considerably smaller than the synthesized results of reference 3 for horizontal-tail locations one-quarter and three-quarters of the vertical-tail span above the base of the vertical tail (locations B and D).

CONCLUSIONS

The results of the investigation to determine the effects of horizontal-tail span and vertical location on the aerodynamic characteristics of an unswept tail assembly in sideslip and to check the suitability of using the well-known finite-step method to obtain the span loadings and, hence, the stability derivatives indicate the following conclusions:

1. The use of the finite-step method provided values of the static-lateral-stability derivatives that were in good agreement with experimental results and, in general, appears to provide a simple and effective means for investigating span loadings of intersecting surfaces.

2. The addition of a horizontal tail to the stub-fuselage and vertical-tail combination produced the greatest increase in the magnitude of the lateral-force derivative C_{Y_β} for horizontal-tail locations near either tip of the vertical tail. For horizontal tails located at the top of the vertical tail an increase in horizontal-tail span provided a relatively large additional increase in C_{Y_β} only for horizontal tails having spans less than the span of the vertical tail. Spans larger than the vertical-tail span provided only small additional increases.

3. Horizontal tails of all spans located one-quarter and one-half of the vertical-tail span above the base of the vertical tail produced a decrease in the magnitude of the lateral-force derivative C_{Y_β} of the horizontal-tail-off configuration.

4. Variations in both horizontal-tail span and vertical location produced a strong influence on the rolling-moment derivative of the horizontal tail.

5. The greatest variation of the rolling-moment derivative of the complete tail assembly with horizontal-tail span occurred for the horizontal tail located at the top of the vertical tail.

6. The end-plate effect of the horizontal tail, calculated by means of the finite-step method and expressed in terms of the ratio of effective aspect ratio to geometric aspect ratio, indicated a greater influence of horizontal-tail span than that obtained from the synthesized results by using the minimum-induced-drag and lifting-line theories. The end-plate effect indicated by the finite-step method was smaller for horizontal-tail locations near the quarter and three-quarter vertical-tail-span positions than the effect indicated by the synthesized results.

LANGLEY AERONAUTICAL LABORATORY,
NATIONAL ADVISORY COMMITTEE FOR AERONAUTICS,
LANGLEY FIELD, VA., *December 24, 1952.*

APPENDIX A

EFFECT OF NUMBER OF HORSESHOE VORTICES

The finite-step method, as the name implies, approximates the spanwise loadings of the vertical and horizontal tails by means of step loadings with the number of steps, of course, corresponding to the number of horseshoe vortices used to define the configuration. In order to obtain an indication as to the number of horseshoe vortices that should be used to obtain reasonably accurate results, especially in regard to the total load carried by the surface, calculations were performed for a rectangular-plan-form wing of aspect ratio 2 to determine the finite-span lift-curve slope C_{L_α} for various numbers of horseshoe vortices distributed across the span. The calculations were made for a wing rather than for a tail configuration since the computations were much simpler and the results were more quickly obtained. The calculated results are presented in figure 15 and are compared with a lifting-surface theory. With four horseshoe vortices, a value of C_{L_α} approximately 15 percent higher than that for the lifting-surface theory is obtained. By using eight vortices, this difference is reduced to about 6 percent and, with 12 vortices, to about 3 percent.

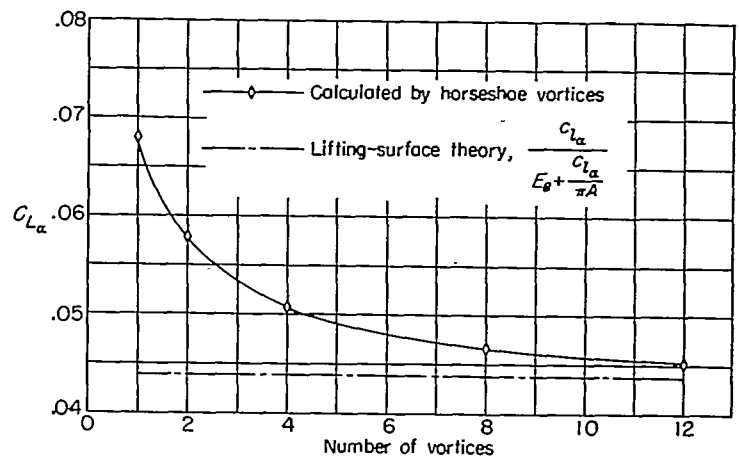

FIGURE 15.—Calculated results for the lift-curve slope C_{L_α} for a rectangular-plan-form wing of aspect ratio 2 for various numbers of horseshoe vortices distributed across the span compared with lifting-surface theory. $\left(\text{Calculations valid only for } c_{l_\alpha}=\frac{2\pi}{57.3}.\right)$

A more complete comparison is presented in figure 16 which shows C_{L_α} for a rectangular wing as a function of aspect ratio for several different numbers of horseshoe vortices distributed across the span. Using four horseshoe vortices at the higher aspect ratios gives results comparable to lifting-line theory. At the low aspect ratios, however, the finite-step method produces more accurate results than the lifting-line theory. Using a larger number of vortices, such as eight or more, appears to provide results approaching lifting-surface-theory values. The use of more than eight horseshoe vortices seems to be desirable only if a well-defined spanwise loading curve is needed. Figure 16 shows that the minimum number of vortices that can be employed to obtain reasonably accurate results is four. For the calculations of the various tail configurations presented, four horseshoe vortices appear to be the most practical to use in view of the accuracy obtained and the additional computational time that would be required if this number were increased.

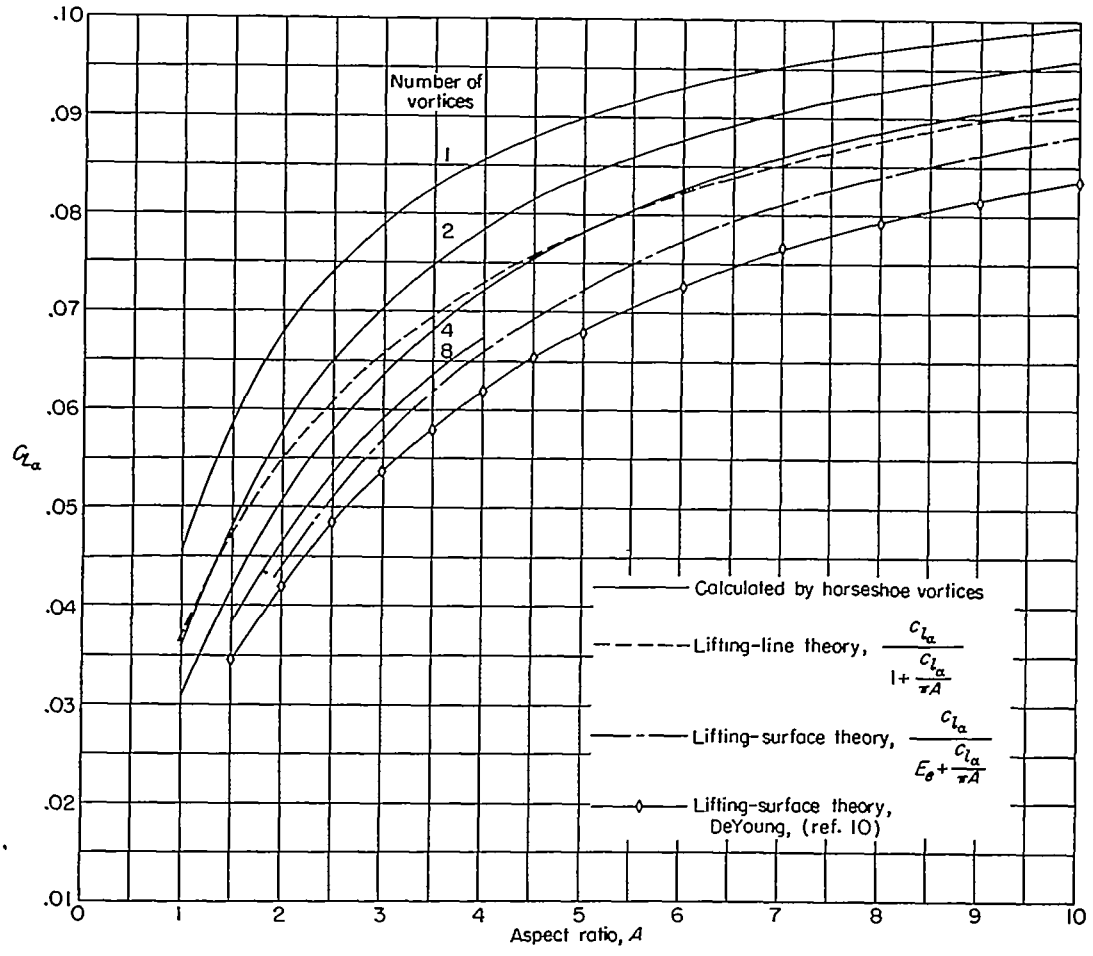

FIGURE 16.—Chart of lift-curve slope C_{L_α} against aspect ratio A for various numbers of horseshoe vortices across the span of a rectangular-planform wing compared with lifting-line theory, lifting-surface theory, and values obtained from reference 10. $\left(\text{Chart valid only for } c_{l_\alpha}=\frac{2\pi}{57.3}.\right)$

APPENDIX B

FUSELAGE EFFECT

Before any comparison between calculated and experimental results can be effected, some representation of the fuselage must be introduced into the calculations. Several attempts were made to calculate the approximate effect of the fuselage by means of horseshoe vortices and the results are presented in figure 17. The criterion chosen as a basis for selecting a representation of the fuselage was reasonable agreement between calculated and experimental values of C_{Y_β} for the vertical-tail—fuselage combination. Since the vertical tail was previously considered to extend to the fuselage center line, two half-span horseshoe vortices were incorporated into the calculations. The half-span vortices were chosen since the maximum fuselage width was 5 inches. The results provided an increase in the magnitude of C_{Y_β}; however, a comparison with the experimental C_{Y_β} indicated the increase to be insufficient. An attempt to increase the end-plate effect by extending the end-plate chord provided an almost negligible increase in C_{Y_β} as compared with the previous case. Since both calculated values are about 10 percent less than the experimental values in magnitude, a half-span vortex was included to represent the fuselage depth, the final fuselage representation resulting in a T-shaped cross section. Although this case provided sufficient agreement with the experimental C_{Y_β}, the value of C_{l_β} was in poorer agreement with experimental value than for the vertical tail with no fuselage considered.

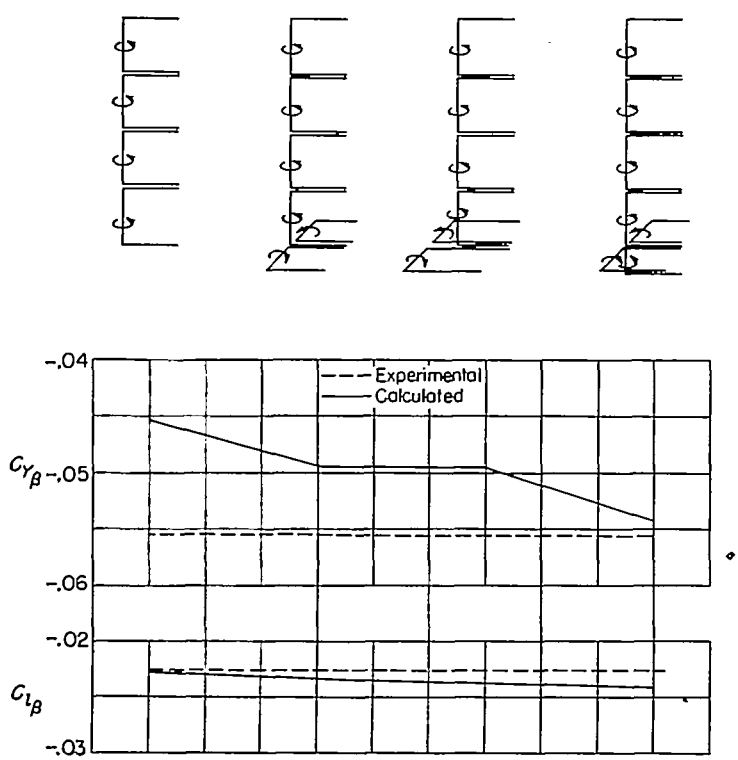

FIGURE 17.—Comparison of experimental results of the stub-fuselage—vertical-tail combination with several calculated fuselage—vertical-tail configurations employing horseshoe vortices to approximate the fuselage effect.

Several additional attempts to calculate the fuselage effect such as using the flow around an infinite cylinder and using several sources and sinks to represent the fuselage provided a poorer agreement with the experimental value of C_{Y_β} for comparable unknowns than using the T-shaped fuselage representation. Since the T-shaped fuselage appeared to give the best comparison with the experimental value of C_{Y_β} for the fuselage—vertical-tail combination, it was used to estimate fuselage effect for horizontal-tail-on configurations in the following manner. Calculations were performed for the vertical tail with the 10-inch horizontal tail attached and the T-shaped fuselage present for all vertical locations of the horizontal tail. Fuselage increments, obtained by subtracting the calculated values for the fuselage-off configuration from those for the fuselage-on configuration at each vertical location of the horizontal tail, gave the correct increments for the 10-inch tail configurations. These increments were then added to all other values calculated for the horizontal- and vertical-tail configurations. The increments ΔC_{Y_β} and ΔC_{l_β} thus obtained are presented in figure 18. A special case was obtained for location A since the horizontal tail was considered to extend through the fuselage. For this case, the fuselage was represented by only a half-span vortex to account for fuselage depth. It should be pointed out that the results presented in figures 17 and 18 have the same section-lift-curve-slope correction applied as that discussed in the section entitled "Comparison of Calculated and Experimental Results."

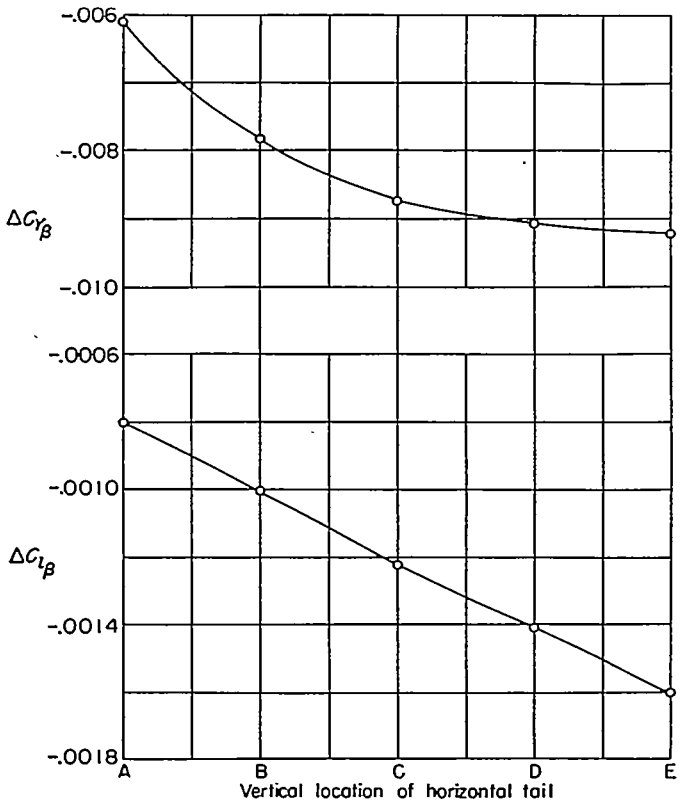

FIGURE 18.—Calculated increments of fuselage effect for configurations having the 10-inch horizontal tail at various vertical locations.

REFERENCES

1. Rotta, J.: Luftkräfte am Tragflügel mit einer seitlichen Scheibe. Ing.-Archiv, Bd. XIII, Heft 3, June 1942, pp. 119–131.
2. Katzoff, S., and Mutterperl, William: The End-Plate Effect of a Horizontal-Tail Surface on a Vertical-Tail Surface. NACA TN 797, 1941.
3. Murray, Harry E.: Wind-Tunnel Investigation of End-Plate Effects of Horizontal Tails on a Vertical Tail Compared With Available Theory. NACA TN 1050, 1946.
4. Lyons, D. J., and Bisgood, P. L.: An Analysis of the Lift Slope of Aerofoils of Small Aspect Ratio, Including Fins, With Design Charts for Aerofoils and Control Surfaces. R. & M. No. 2308, British A.R.C., 1945.
5. Gray, W. L., and Schenk, K. M.: A Matrix Solution for the Steady State Aeroelastic Loading on Wings (Rough Draft). Document No. D 10624, Boeing Aircraft Co., Mar. 24, 1950.
6. Weissinger, J.: The Lift Distribution of Swept-Back Wings. NACA TM 1120, 1947.
7. Glauert, H.: The Elements of Aerofoil and Airscrew Theory. Second ed., Cambridge Univ. Press, reprint of 1948, p. 158.
8. Van Dorn, Nicholas H., and DeYoung, John: A Comparison of Three Theoretical Methods of Calculating Span Load Distribution on Swept Wings. NACA TN 1476, 1947.
9. Diedrich, Franklin W.: Charts and Tables for Use in Calculations of Downwash of Wings of Arbitrary Plan Form. NACA TN 2353, 1951.
10. DeYoung, John, and Harper, Charles W.: Theoretical Symmetric Span Loading at Subsonic Speeds for Wings Having Arbitrary Plan Form. NACA Rep. 921, 1948.
11. Jacobs, Eastman N., and Abbott, Ira H.: Airfoil Section Data Obtained in the N.A.C.A. Variable-Density Tunnel as Affected by Support Interference and Other Corrections. NACA Rep. 669, 1939.